Article

JOURNAL OF COMPOSITE MATERIALS

Journal of Composite Materials
0(0) 1–11

DOI: 10.1177/0021998312463107
jcm.sagepub.com

SAGE

Fluorescent electrospun polyvinyl alcohol/CdSe@ZnS nanocomposite fibers

Emre Atabey[1], Suying Wei[2], Xi Zhang[1], Hongbo Gu[1,3], Xingru Yan[1], Yudong Huang[3], Lu Shao[3], Qingliang He[1], Jiahua Zhu[1], Luyi Sun[4], Ashwini S Kucknoor[5], Andrew Wang[6] and Zhanhu Guo[1]

Abstract

Uniform and bead-free polyvinyl alcohol (PVA) and its nanocomposite fibers filled with different loadings of CdSe@ZnS quantum dots (QDs) were prepared by the electrospinning process. The incorporation of QDs into PVA solution lowered the viscosity of the system. The electrospinning parameters, including applied voltage, feed rate, and working distance were optimized to prepare high quality nanocomposite fibers. Increasing the voltage from 20 to 25 kV, the average diameter of PVA fibers reduced from ca. 284 to 164 nm (42.5% decrease) and the average diameter of PVA/QDs nanocomposite fibers decreased from ca. 365 to 240 nm (34.2% decrease). The PVA/QDs (5.0 wt%) nanocomposite fibers were examined under a fluorescent microscopy. The thermal stability was investigated by both thermogravimetric analysis and differential scanning calorimetry. Fourier transform infrared spectroscopy was utilized to characterize the functionality of the fibers and to investigate the interaction between PVA and inorganic additions. Unique fluorescent phenomenon was observed in the PVA fibers after incorporation of small amount of QDs.

Keywords

Polyvinyl alcohol, quantum dots, electrospinning, nanofibers, rheological behavior, fluorescence

Introduction

Polyvinyl alcohol (PVA) is a water soluble semi-crystalline polymer that has been well studied.[1,2] Among different forms of PVA products, PVA fibers are widely used for industrial applications[3–5] because of their high chemical and thermal stability, excellent mechanical properties, and low manufacturing cost.[6–10] Recently, the fabrication of PVA fibers by electrospinning has been explored.[4,11–14] Huge efforts have been made to improve the quality of PVA fibers. The electrospun fibers with small diameters have a large specific surface area and a high aspect ratio, which are useful for a variety of applications, including separation membranes, artificial blood vessels.[15]

Quantum dots (QDs) are defined as particles with physical dimensions smaller than the exciton Bohr radius,[16–20] at which length scale the addition or removal of an electron can change the properties significantly because of the quantum effects arising from the confinement of electrons and holes inside. Size influences certain properties of QDs, such as electrical and nonlinear optical properties, making them greatly different from their bulky counterparts.[21] One of the most unique properties of QDs is their band gap tunability, i.e. the wavelength at which they will absorb or emit radiation can be adjusted. The larger the size, the longer the wavelength of light absorbed

[1]Integrated Composites Laboratory (ICL), Dan F. Smith Department of Chemical Engineering, Lamar University, Beaumont, TX77710, USA
[2]Department of Chemistry and Biochemistry, Lamar University, Beaumont, TX77710, USA
[3]School of Chemical Engineering and Technology, Harbin Institute of Technology, 150001China
[4]Department of Chemistry and Biochemistry, Texas State University-San Marcos, San Marcos, TX, 78666, USA
[5]Department of Biology, Lamar University, Beaumont, TX77710, USA
[6]Ocean NanoTech, LLC, 2143 Worth Ln., Springdale, AR72764, USA

Corresponding author:
Zhanhu Guo, Ocean NanoTech, LLC, 2143 Worth Ln., Springdale, AR72764, USA.
Email: zhanhu.guo@lamar.edu

and emitted. Another advantage of QDs is that they can be molded into a variety of different forms, such as sheets or three-dimensional arrays, in contrast to the traditional semiconductive materials, which are crystalline and rigid.[22] They can be easily mixed with organic polymers, dyes, or made into porous films.[23]

Colloidal semiconductive QDs have the potential to overcome the problems encountered by the traditional organic fluorophores, by combining the advantages of readily tunable spectral properties (with broad excitation spectrum and narrow emission bandwidths).[24] With a high photo bleaching threshold, good chemical stability and large absorption coefficients across a wide spectral range.[25–27] QDs are playing more important role as versatile labels for optoelectronics, tissue engineering and for biomarkers.[28,29] Fluorophores deposited on surfaces or embedded in dielectric particles were shown to display different radiative decay rates, quantum yields and photobleaching rates.[30,31]

Polymer nanocomposites (PNCs) have attracted great interests due to their wide applications arising from their unique physicochemical properties.[3,4,32,33] As an important water soluble polymer, PVA has been utilized to fabricate PNCs for applications in various fields.[34] For example PVA nanocomposites containing the designed QDs are promising for biological, optoelectronic, and photonic applications. Electrospinning serves as a highly efficient method to produce PVA based nanocomposite fibers.[35–38] Over the past few years, many researchers have investigated various parameters affecting the morphology and the diameters of the electrospun PVA fibers, e.g., solution concentration, solution flow rate, degree of hydrolysis, applied electrical potential, collection distance, but often, conflicting results were observed.[39] However, the fluorescent PVA nanofibers with QDs have not been reported yet.

In this study, fluorescent PVA nanocomposite fibers containing different loadings of QDs were prepared by electrospinning. The electrospinning operation parameters, including spinning voltage, feed rate, and working distance (tip-to-collector distance) were optimized. The physicochemical properties of the PVA nanocomposite fibers containing QDs were examined with scanning electron microscopy (SEM), differential scanning calorimetry (DSC), thermogravimetric analysis (TGA), and fluorescence microscope.

Experimental

Materials

PVA (molecular weight 89,000–98,000, degree of polymerization 2000–2200) was purchased from Sigma-Aldrich. Core/shell cadmium selenide (CdSe)/zinc sulfide (ZnS) quantum dots (QDs, ~5 nm) coated with octadecylamine were supplied by Ocean NanoTech LLC. All the chemicals were used as received without any further treatment.

Polymer solution preparation

The PVA solution was prepared by dissolving PVA powders (10.0 g) in deionized water (90.0 g). After 2 h of magnetic stirring at 50°C, a 10 wt% transparent PVA aqueous solution was formed. QDs aqueous solution (0.9 mL, 1.1 g QDs/100 g solution) was added into PVA solution to obtain a loading of 1.0 wt% QDs in PVA. QDs with a concentration of 1 and 5 wt% were added into the pure PVA solution, respectively.

Electrospinning setup

The electrospinning was performed on a home-made set up, which was detailed in previous reports.[40] The polymer solution was dispensed via a stainless-steel needle (inner diameter 0.60 mm) connected to a high-voltage power supply (Gamma High Research, Product HV power Supply, Model No.ES3UP-5w/DAM), which was in the range 0–30 kV. The polymer solution in a 5 mL syringe was ejected by a syringe pump (NE-300, New Era Pump Systems, Inc.) with an adjustable feed rate. The electrically grounded aluminum foils served as a collecting electrode. The working distance, electrical voltage, and feed rate were optimized for spinning high quality nanocomposite fibers.

Characterization

Scanning electron microscopy (SEM, Hitachi S-3400) was used to investigate the morphologies of pure PVA and its nanocomposite fibers with various QDs loadings. PVA/QDs nanocomposite fiber was examined by a fluorescent microscope. The nanofibers with embedded QDs were immobilized on a clean microscope slide and observed under oil-immersion using an Olympus BX-31 epifluorescence microscope equipped with a DP-72 camera. Images were obtained using Olympus CellSens software.

The rheological behaviors of the PVA solution and PVA/QDs dispersions with different QDs loadings were examined with a rheometer (TA Instruments, AR 2000ex). The shear rate changed from 1.0 to 1200 rad/s at 25°C. Measurements were applied in a cone and plate geometry with a diameter of 40 mm and a truncation of 66 μm.

Both thermal gravimetric analysis (TGA) and differential scanning calorimetric (DSC) analysis were performed to investigate the thermal properties of PVA and its nanocomposite fibers. The TGA experiments

were carried out using a TA Instruments Q500 analyzer under a heating rate 20°C/min and an air flow rate of 50 mL/min from 25 to 800°C. Differential scanning calorimeter (DSC, TA Instruments Q2000) was used to obtain DSC thermograms. Each sample was first heated to 250°C with a heating rate of 10°C/min to remove thermal history, followed by cooling down to 40°C at a rate of 10°C/min to record crystallization temperature, and then reheat to 250°C at the same rate to determine the melt temperature. The experiments were carried out under a nitrogen purge (20 mL/min).

Fourier transform infrared (FT-IR, Bruker Tensor 27) spectrophotometer with hyperion 1000 attenuated total reflectance (ATR) microscopy accessory was used to characterize PVA and its nanocomposite fibers over the range of 500 to 4000/cm at a resolution of 4/cm.

Results and discussion

Voltage effect

An important parameter in electrospinning is the applied voltage which controls the surface charge on the polymer solution jet. When a high voltage is applied to a liquid droplet, the body of the liquid becomes charged. The resulting electrostatic repulsion causes equilibrium among the surface tension and the droplet is stretched. At a critical point, a stream of liquid erupts from the surface.[4,41] Figure 1 shows the SEM images of PVA and its nanocomposite fibers containing 1.0 wt% QDs electrospun at two different applied voltages, 20 and 25 kV, which appeared to be the top and bottom limit of the processing window at a flow rate of 10 μL/min and a working distance of 10.0 cm. When increasing the voltage from 20 to 25 kV, the average diameter of PVA fibers reduced from ca. 284 to 164 nm (42.5% decrease) and the average diameter of PVA/QDs nanocomposite fibers decreased from ca. 365 to 240 nm (34.2% decrease). The above observation is expected, since a higher applied voltage would result in an enhanced electrostatic force on the solution jet, resulting in thinner fibers.[42] The addition of QDs to the PVA solution was observed to reduce the bead formation and to increase the fiber diameter, because it is essential for QDs in polymer solution to obtain an accumulation of solution concentration according to a power law relationship.[43,44] In addition, electrospinning from high QDs concentration of polymer solution has been explored to produce a bimodal distribution of fiber sizes, reminiscent of distributions observed in the similar droplet generation process of electrospinning. Furthermore, the electrostatic effects influence the macroscale morphology of the electrospun fibers in the formation of 3-D structures.[45,46]

Feed rate effect

As the feed rate increases, more polymers are available at the needle tip to be electrospun, which at some point

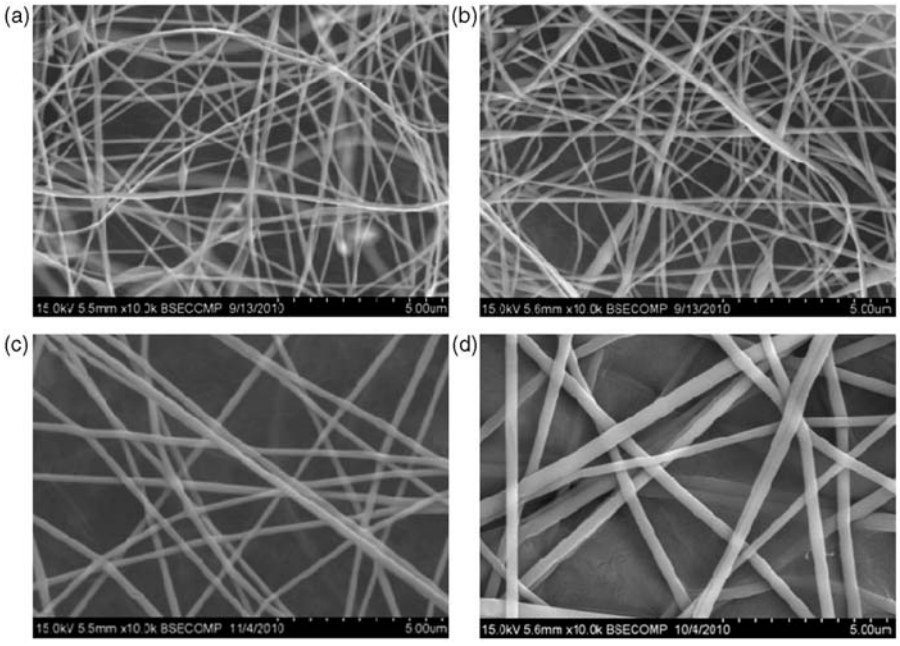

Figure 1. SEM images of pure PVA fibers with an applied voltage of (a) 25 kV, (b) 20 kV; and PVA/QDs (1.0%) nanocomposite fibers with an applied voltage of (c) 25 kV, (d) 20 kV.

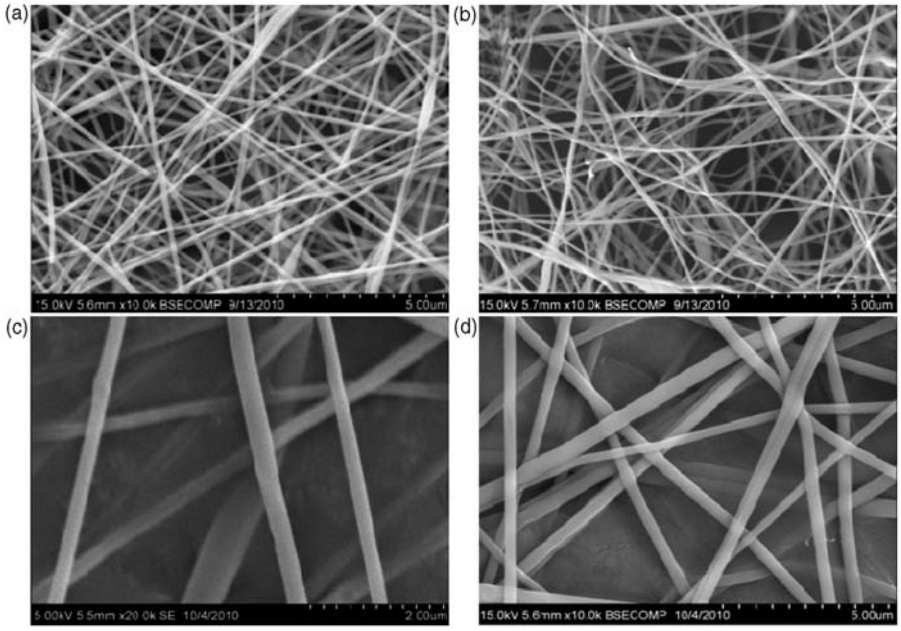

Figure 2. SEM images of PVA and PVA/QDs (1.0%) nanocomposite fibers under different feed rates: (a) 0% QDs, 25 kV, 12 μL/min; (b) 0% QDs, 20 kV, 8 μL/min; (c) 1.0% QDs, 25 kV, 12 μL/min; (d) 1.0% QDs, 20 kV, 10 μL/min.

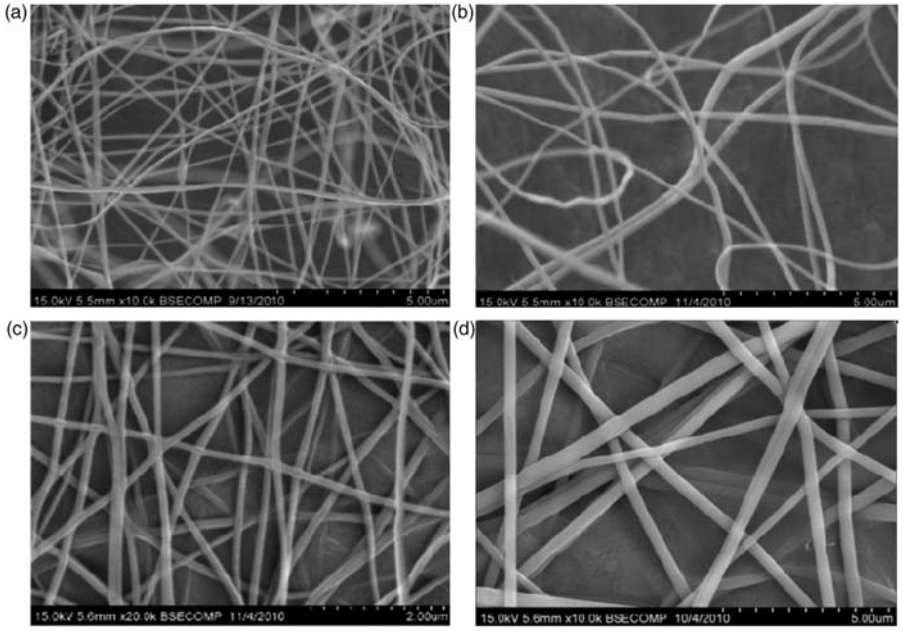

Figure 3. SEM images of PVA and PVA/QDs (1.0%) nanocomposite fibers with different working distances: (a) 0% QDs, 12 cm; (b) 0% QDs, 10 cm; (c)1% QDs, 12 cm; (d) 1% QDs, 10 cm.

will exceed the rate of removal at a fixed electric field and nonuniform drawing takes place resulting in beaded nanofibers.[47] Figure 2 shows the SEM images of fibers produced at a fixed working distance of 10.0 cm with applied voltages (20 and 25 kV) and feed rates (8, 10 and 12 μL/min). When the feed rate was increased from 8 to 12 μL/min for PVA fibers and 10 to 12 μL/min for nanocomposite, the average diameter of PVA fibers and its QDs nanocomposite fibers increased from ca. 172 to 176 nm (2.3% increase) and

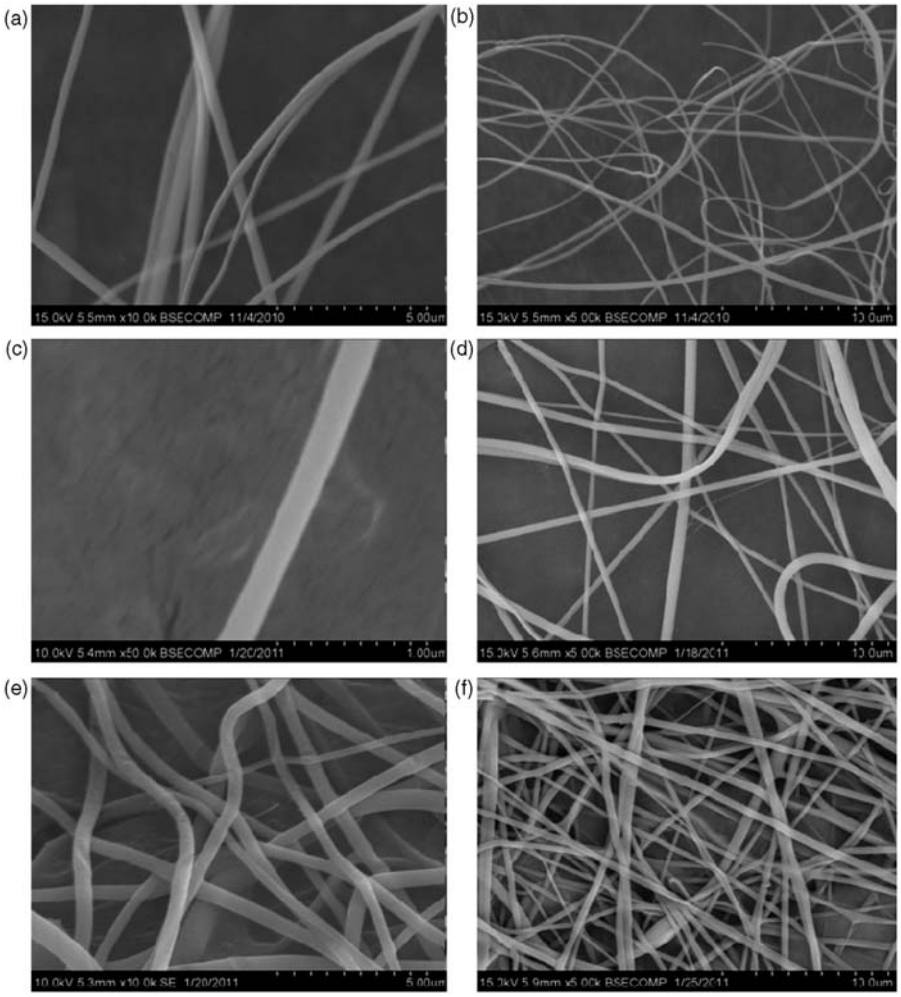

Figure 4. SEM images of (a) 0% QDs, 4.5 μL/min; (b) 0% QDs, 3.5 μL/min; (c) 1.0% QDs, 4.5 μL/min; (d) 1% QDs, 3.5 μL/min; (e) 5.0% QDs, 4.5 μL/min; (f) 5% QDs, 3.5 μL/min.

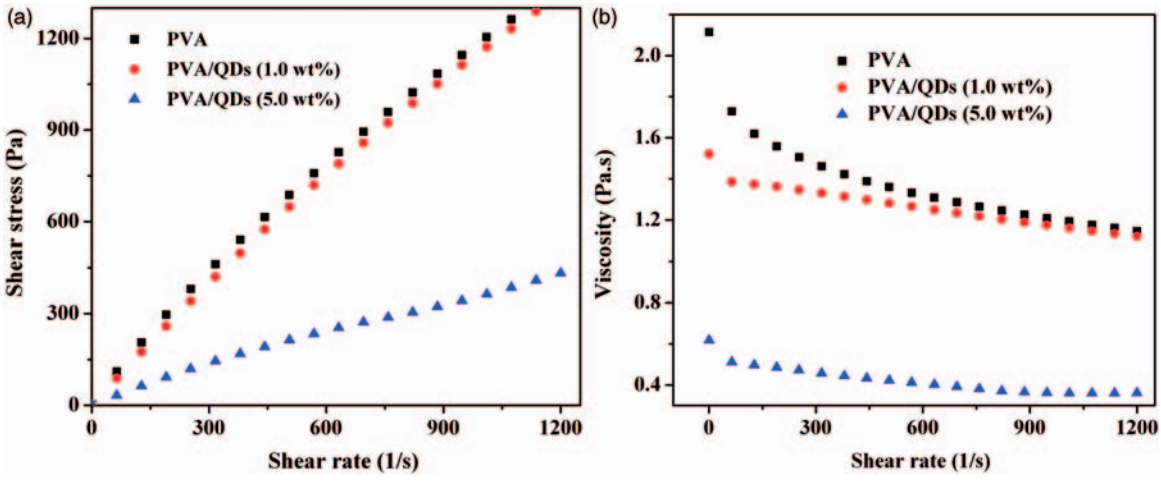

Figure 5. (a) Shear stress vs. shear rate and (b) viscosity vs. shear rate of neat PVA solution and PVA/QDs dispersions.

from ca. 365 to 442 nm (21.1% increase), respectively. The results show that the diameter size and uniformity of the electrospun PVA fibers were not significantly influenced by the feed rate. Once the feed rate was sufficient to form continuous fibers, a higher feed rate would lead to larger fiber diameter or even generate beads.[35,48,49] Here, uniform fibers are still observed even at a flow rate of 12 μL/min, which favors fiber production with a larger yield.

Working distance effect

Working distance, the distance between the needle tip and the aluminum foil, was reported to have a significant influence on the morphology of the formed fibers.[50] When the working distance is reduced, the electric field strength increases, leading to an enhancement of the acceleration of the jet to the collector.[51] At a constant feed rate of 10 μL/min and voltage of 20 kV, the working distance was adjusted from 10.0 to 12.0 cm to produce fibers. As shown in Figure 3, the average diameter of the electrospun PVA fibers increased from 174 nm (12.0 cm working distance) to 186 nm (10.0 cm working distance). But the electrospun fibers turned to be more uniform at 12.0 cm working distance. The poor fiber uniformity and formation of beads were due to the shorter working distance induced larger electrostatic force, leading to unbalanced forces on jet flow.[40] The average diameters of PVA/QDs nanocomposite fibers changed from 442 to 317 nm when increasing the working distance from 10.0 to 12.0 cm. The addition of QDs in the PVA solution lead to a decrease in solution viscosity, which leads to fewer beads and more uniform fibers.[52,53]

Effect of QDs concentration

The major effect of the QDs concentration on the resultant fiber diameters is expected to come from the corresponding large variations in viscosity and viscoelestic responses of the PVA/QDs dispersions. An appropriate polymer concentration is necessary to obtain uniform fibers. Generally, an elevated QDs concentration may lead to difficulty in the electrospinning process, eventually making it impossible to spin continuous fibers due to the lowered viscosity. Therefore, the deliberated control of QDs concentration is crucial for the final nanofiber products.

Figure 4 shows the SEM images of the samples prepared under a working distance of 14.0 cm and an applied voltage of 20 kV. The PVA nanocomposite fibers containing 1.0 wt% QDs exhibit better diameter uniformity than the pure PVA fibers. However, PVA/QDs (5.0 wt%) nanocomposite fibers were observed to be thicker in diameter with beads on nanofibers. As seen in SEM images (at a flow rate of 4.5 μL/min), the average diameters of the electrospun PVA/QDs (1.0 wt%) and PVA/QDs (5.0 wt%) nanocomposite fibers are ca. 310 and 420 nm, respectively. With a lower flow rate of 3.5 μL/min, their diameters changed to be 290 and 380 nm, respectively. The more viscous solution (lower than the process limiting concentration) is found to form more uniform fibers.

The effect of QDs concentration on the polymer solution influenced the electrospun nanofibers.[41] The reduction of the nanofiber diameter is achieved by lowering the QDs concentration on the PVA solution.[54]

Rheological behaviors

Figure 5 shows the shear stress and viscosity as a function of shear rate for 10.0 wt% PVA solution, and PVA/QDs dispersions. The pure PVA solution was more viscous than the PVA/QDs dispersions. With 1.0 wt% QDs, the dispersion exhibited slightly lower viscosity than the pure PVA solution. However, the incorporation of 5.0 wt% QDs led to a dramatic decrease in viscosity. In this work, the long alkyl chains of octadecylamine coated on the QDs surface provide proper particle spacing with a uniform particle suspension through steric hindrance, which reduces the tendency towards uncontrolled flocculation and leads a decreased viscosity.

As the shear rate reached 1200/s, the viscosity of 10.0 wt% PVA solution dropped from 2.12 to 1.15 Pa·s. PVA solution and PVA/QDs dispersions have been modeled using a power law equation (1).[55,56]

$$\tau = K\left(\frac{\partial u}{\partial y}\right)^{n} \quad (1)$$

where τ is the shear stress, K is the flow consistency index, $\left(\frac{\partial u}{\partial y}\right)$ is the shear rate, and the value n determines the flow behavior. For Newtonian fluids, $n = 1$, and for pseudoplastic fluids, $n < 1$. The values of n and K are listed in Table 1. The less viscous fluid has a greater ease of movement as compared to the more viscous fluid.[57] The K values can be usually related to the fluid viscosity. And the larger deviation of n from 1, the more non-Newtonian behavior the fluids would follow. In Table 1, the K values vary quite consistently

Table 1. The values of n and K for pure PVA solution and PVA/QDs dispersions

Solutions	n	K
Pure PVA	0.822	4.118
PVA/QDs (1.0 wt%)	0.871	2.823
PVA/QDs (5.0 wt%)	0.819	1,279

with the viscosity curves depending on the QDs loading, as shown in Fig. 5. It was observed that the solutions filled with 1 wt% QDs show the highest n value (>0.87), which means these solutions show more Newtonian behavior and n is less dependent on the $\left(\frac{\partial u}{\partial y}\right)$. The relatively flat curves, especially at higher $\left(\frac{\partial u}{\partial y}\right)$, for 5 wt% QDs in Fig. 5 indicate a tendency of these fluids from non-Newtonian to Newtonian behavior. These fluid behavior changes are essentially important in electrospinning process for choosing the optimal operation conditions, such as feed rate and applying voltage.

Thermal properties

Figure 6 shows the TGA thermograms of powder PVA, dry QDs, PVA fibers, and PVA/QDs nanocomposite fibers with different QDs loadings. The major weight loss of powder PVA occurred between 190 and 440°C, which is dominated by the decomposition of the side chain of PVA.[37] Nanofibers of 10 wt% PVA starts losing weight at about 100°C from the evaporation of water. Nanofibers included QDs nanoparticles with transition starting at about 130–700°C.[58] Some of the 10 wt% PVA with 1 wt% QDs weight loss were observed in the range of 50 to 250°C and then followed by a larger weight loss in the range of 250 to 580°C, on which QDs were left at about 600°C.[59] The nanostructure of QDs is critical to improve the thermal stability of nanocomposites. When 10 wt% PVA with 5 wt% QDs is heated, drying process takes place firstly. Further heating removes new amount of water from chemical reactions through thermo-condensation process, which occurs at temperature above 160°C. As the temperature increases, the evaporation rate of water in the material becomes higher, thus the weight loss increases. One-half of the 10 wt% PVA with 1 wt% QDs weight loss observed in the range of 50 to 200°C and then followed by a further smaller weight loss in

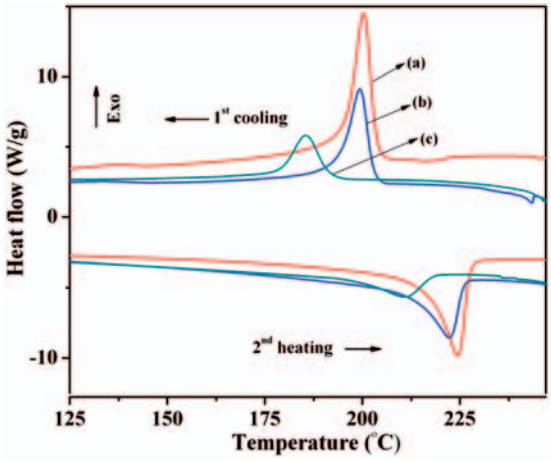

Figure 7. DSC thermograms of the thin film samples cast from the solutions to spin fibers (a) 10.0 wt% PVA; (b) PVA/QDs (1.0 wt%); (c) PVA/QDs (5.0 wt%).

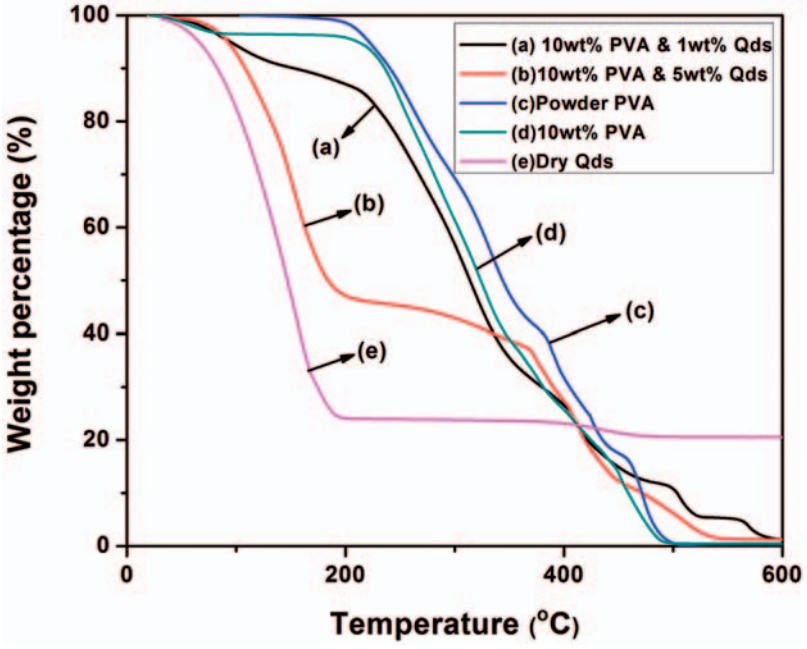

Figure 6. TGA thermograms of powder PVA, dry QDs, PVA fibers, and PVA/QDs nanocomposite fibers with different QDs loadings.

Table 2. Thermal properties and calculated crystallinity of pure PVA and PVA/QDsws

Material	T_m (°C)	H_m (J/g)	T_c (°C)	H_c (J/g)	Crystallinity (%)
10 wt% PVA	224.4	50.88	200.3	73.25	52.8
PVA/QDs (1.0 wt%)	222.4	37.30	199.3	46.22	33.3
PVA/QDs (5.0 wt%)	211.4	11.11	185.5	22.27	16.0

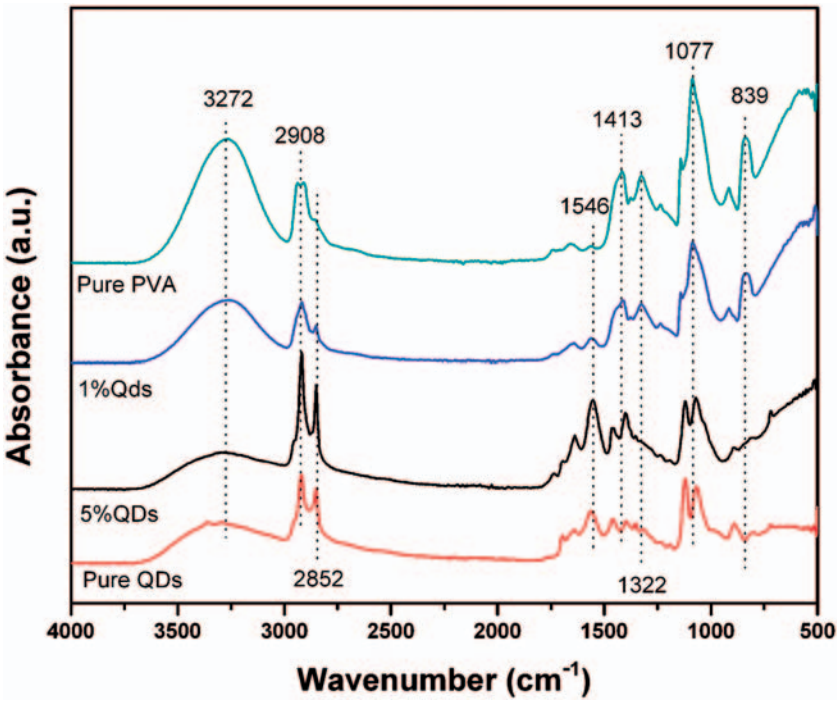

Figure 8. FT-IR spectra of PVA fibers, dried CdSe-ZnS QDs, PVA/QDs (1.0 wt%) and PVA/QDs (5.0 wt%) nanocomposite fibers.

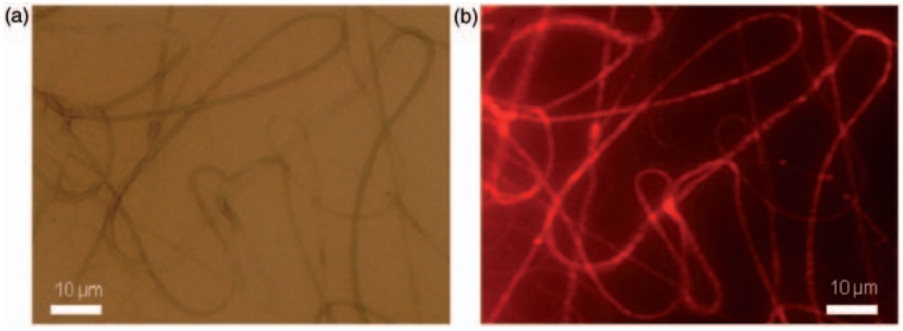

Figure 9. Fluorescence microscopy images of PVA/QDs composite nanofiber in (a) Bright field; (b) Dark field.

the range of 200 to 400°C, QDs were left at about 600°C.

PVA is a semi-crystalline polymer exhibiting both crystallization temperature (T_c) and melting temperature (T_m). The heating run was used to obtain the melting temperature and melting enthalpy, while the cooling run was used to characterize the crystallization behavior. A relatively large and sharp endothermic curve is observed, while the crystallization peak of PVA became broader and shifted to lower temperature. The melting peaks for pure PVA and PVA/QDs appeared at around 225°C, representing the melting of the crystalline

PVA phase. The melting temperature depression was caused by morphological changes, which involved the thickness of the crystallites and the degree of crystallinity. The melting enthalpy (ΔH_m, based on the weight of pure polymer rather than the total weight of polymer nanocomposites) was observed to decrease significantly from 50.88 to 37.30 J/g and 11.11 J/g, which is consistent with the PVA nanocomposite fibers containing silver nanoparticles.[3] This is due to the reduced mobility of the polymer chains after being attached to the nanoparticle surface. The nanoparticle is also observed to have a significant effect on the melting temperature and the melting enthalpy, Table 2.

The degree of crystallinity of the PVA can be estimated using Equation (2)[60,61]:

$$X_c = \frac{\Delta H_f}{\Delta H_f^o} \quad (2)$$

where ΔH_f is the measured enthalpy of fusion from the DSC thermogram (based on the weight of pure polymer rather than the total weight of polymer nanocomposites), and ΔH_f^o is the enthalpy of fusion of 100% crystalline PVA (ΔH_m is 138.6 J/g).[1,61] The crystallinity of 10 wt% PVA is higher than the other samples. More QDs in PVA the solution makes it less crystalline.

FT-IR analysis

FT-IR analysis was conducted to study the potential chemical interactions between the PVA and QDs in the fibers. Figure 8 shows the FT-IR spectra of the dried QDs, pure PVA fibers, and PVA/QDs nanocomposite fibers. All the samples have characteristic C-H stretch peaks at ca. 839 and 2914/cm, and $-CH_2$ stretch peaks at 1322/cm (weaker bond for pure QDs and PVA/QDs (5.0 wt%)).[62] The peaks exhibited higher intensity in the dried QDs samples and weaker inthe polymer nanocomposites. Both –OH stretch peaks[63,64] (3285 and 1650/cm), C–C stretch peaks (1413/cm) and C–O stretch peaks (839, 1077 and 1322/cm) were found stronger in both PVA and nanocomposites, and weaker in the evaporated QDs sample.[65] In PVA molecules, hydroxyl groups are grafted to the backbone. The QDs sample has a weak response to –OH group through the hydrogen bonding. A strong –COOH stretch peak at 1546/cm was observed in the dried QDs sample, but not in the PVA/QDs nanocomposites.[66] These differences indicate an interaction between QDs and the polymer matrix.

Fluorescent microscopy

Fluorescent microscopy images were captured from the same spot of the electrospun samples with and without UV excitation as shown in Figure 9. When the PVA/QDs (5.0 wt%) nanocomposite fibers were examined under a fluorescent microscopy, they were visible under both visible light and UV light excitation. QDs nanofibers are fluorescent with excitation from the UV light. There were also bright spots on the fibers, which are believed to be the regions with relatively high concentrations of QDs.[67]

Conclusion

In summary, the optimum condition to produce the bead-free and uniform PVA nanofibers via electrospinning was investigated. QDs were added in PVA aqueous solution which had a significant effect on the quality of fibers. The results have shown that the applied voltage, feed rate and working distance are crucial for tuning the morphology of fibers. Under relatively low concentration of QDs in PVA solution; the viscosity of the solutions decreases slightly. TGA is conducted and the results demonstrate an enhanced thermal stability of the PVA/QDs nanofibers compared to that of the pure polymer fibers. Higher thermal decomposition temperature is also observed in the PVA/QDs nanofibers at a higher particle loading. Therefore, the addition of QDs favors the cross-linkage of PVA matrix resulting in a lower melting temperature and a subsequent improvement in the thermal stability. Unique fluorescent phenomenon was observed in the PVA fibers after incorporation of small amount of QDs.

Funding

This project is financially supported by the National Science Foundation–Chemical and Biological Separations (EAGER:CBET 11-37441) managed by Dr Rosemarie D Wesson.

Acknowledgement

This work was partially supported by the research start-up funds from Lamar University.

Conflict of Interest

None declared.

References

1. DeMerlis CC and Schoneker DR. Review of the oral toxicity of polyvinyl alcohol (PVA). *Food Che Toxicol* 2003; 41: 319–326.
2. Koski A, Yim K and Shivkumar S. Effect of molecular weight on fibrous PVA produced by electrospinning. *Mater Lett* 2004; 58: 493–497.
3. Mbhele ZH, Salemane MG, Van Sittert CGCE, Nedeljkovi JM, Djokovi V and Luyt AS. Fabrication and characterization of silver-polyvinyl alcohol nanocomposites. *Chem Mater* 2003; 15: 5019–5024.

4. Li D and Xia Y. Electrospinning of nanofibers: reinventing the wheel? *Adv Mater* 2004; 16: 1151–1170.
5. Agarwal S, Wendorff JH and Greiner A. Use of electrospinning technique for biomedical applications. *Polymer* 2008; 49: 5603–5621.
6. Li D, Wang Y and Xia Y. Electrospinning of polymeric and ceramic nanofibers as uniaxially aligned arrays. *Nano Lett* 2003; 3: 1167–1171.
7. Pinto NJ, Johnson JAT, MacDiarmid AG, Mueller CH, Theofylaktos N, Robinson DC and Miranda FA. Electrospun polyaniline/polyethylene oxide nanofiber field-effect transistor. *Appl Phys Lett* 2003; 83: 4244–4246.
8. Guo Z, Zhang D, Wei S, Wang Z, Karki AB, Li Y, Bernazzani P, Young DP, Gomes J, Cocke D and Ho TC. Effects of iron oxide nanoparticles on polyvinyl alcohol: interfacial layer and bulk nanocomposites thin film. *J Nanopart Res* 2010; 12: 2415–2426.
9. Teo WE and Ramakrishna S. A review on electrospinning design and nanofibre assemblies. *Nanotechnology* 2006; 17: 89–106.
10. Zhang D, Karki AB, Rutman D, Young DP, Wang A, Cocke D, Ho T and Guo Z. Electrospun polyacrylonitrile nanocomposite fibers reinforced with Fe_3O_4 nanoparticles: Fabrication and property analysis. *Polymer* 2009; 50: 4189–4198.
11. Greiner A and Wendorff JH. Electrospinning: a fascinating method for the preparation of ultrathin fibers. *Angew. Chem. Int. Ed* 2007; 46: 5670–5703.
12. Bognitzki M, Becker M, Graeser M, Massa W, Wendorff JH, Schaper A, Weber D, Beyer A, Gölzhäuser A and Greiner A. Preparation of sub-micrometer copper fibers via electrospinning. *Adv. Mater* 2006; 18: 2384–2386.
13. Li D and Xia Y. Fabrication of titania nanofibers by electrospinning. *Nano Lett* 2003; 3: 555–560.
14. Wu H, Zhang R, Liu X, Lin D and Pan W. Electrospinning of Fe, Co, and Ni nanofibers: synthesis, assembly, and magnetic properties. *Chem Mater* 2007; 19: 3506–3511.
15. Doshi J and Reneker DH. Electrospinning process and applications of electrospun fibers. *J Electrostat* 1995; 35: 151–160.
16. Chan WCW, Maxwell DJ, Gao X, Bailey RE, Han M and Nie S. Luminescent quantum dots for multiplexed biological detection and imaging. *Curr Opin Biotechnol* 2002; 13: 40–46.
17. Henglein A. Small-particle research: physicochemical properties of extremely small colloidal metal and semiconductor particles. *Chem Rev* 1989; 89: 1861–1873.
18. Schmid G. Large clusters and colloids. Metals in the embryonic state. *Chem Rev* 1992; 92: 1709–1727.
19. Alivisatos AP. Semiconductor clusters, nanocrystals, and quantum dots. *Science* 1996; 271: 933–937.
20. Nirmal M and Brus L. Luminescence photophysics in semiconductor nanocrystals. *Acc Chem Res* 1999; 32: 407–414.
21. Murray CB, Norris DJ and Bawendi MG. Synthesis and characterization of nearly monodisperse CdE (E = sulfur, selenium, tellurium) semiconductor nanocrystallites. *J Am Chem Soc* 1993; 115: 8706–8715.
22. Mishra P, Vyas G, Harsoliya MS, Pathan JK, Raghuvanshi D, Sharma P and Agrawal A. Quantum dot probes in disease diagnosis. *J Pharm Pharm Sci Rev* 2011; 1: 42–46.
23. Vlasov YA, Yao N and Norris DJ. Synthesis of photonic crystals for optical wavelengths from semiconductor quantum dots. *Adv Mater* 1999; 11: 165–169.
24. Goldman ER, Balighian ED, Mattoussi H, Kuno MK, Mauro JM, Tran PT and Anderson GP. A natural bridge for quantum dot-antibody conjugates. *J Am Chem Soc* 2002; 124: 6378–6382.
25. Fox TG, Kinsinger JB, Mason HF and Schuele EM. Properties of dilute polymer solutions I—Osmotic and viscometric properties of solutions of conventional polymethyl methacrylate. *Polymer* 1962; 3: 71–95.
26. Kenawy ER, Watkins JR, Bowlin GL, Matthews JA, Simpson DG and Wnek GE. Electrospinning of poly(ethylene-co-vinyl alcohol) fibers. *Biomaterials* 2003; 24: 907–913.
27. Ding B, Yamazaki M and Shiratori S. Electrospun fibrous polyacrylic acid membrane-based gas sensors. *Sens Actuators, B* 2005; 106: 477–483.
28. Huang ZM, Zhang YZ, Kotaki M and Ramakrishna S. A review on polymer nanofibers by electrospinning and their applications in nanocomposites. *Compos Sci Technol* 2003; 63: 2223–2253.
29. Wei S, Sampathi J, Guo Z, Anumandla N, Rutman D, Kucknoor A, James L and Wang A. Nanoporous poly(methyl methacrylate)-quantum dots nanocomposite fibers towards biomedical applications. *Polymer* 2011; 52: 5817–5829.
30. Macklin JJ, Trautman JK, Harris TD and Brus LE. Imaging and time-resolved spectroscopy of single molecules at an interface. *Science* 1996; 272: 255–258.
31. Schniepp H and Sandoghdar V. Spontaneous emission of europium ions embedded in dielectric nanospheres. *Phys Rev Lett* 2002; 89: 257403.
32. Zhu J, Wei S, Chen X, Karki AB, Rutman D, Young DP and Guo Z. Electrospun polyimide nanocomposite fibers reinforced with core-shell Fe-FeO nanoparticles. *J Phys Chem. C* 2010; 114: 8844–8850.
33. Wei H, Yan X, Li Y, Wu S, Wang A and Wei S. Hybrid electrochromic fluorescent poly(DNTD)/CdSe@ZnS composite films. *J Phys Chem. C* 2012; 116: 4500–4510.
34. Yamaoka T, Tabata Y and Ikada Y. Comparison of body distribution of poly(vinyl alcohol) with other water-soluble polymers after intravenous administration. *J Pharm Pharmacol* 1995; 47: 479–486.
35. Deitzel JM, Kleinmeyer J, Harris D and Beck Tan NC. The effect of processing variables on the morphology of electrospun nanofibers and textiles. *Polymer* 2001; 42: 261–272.
36. Sun Z, Zussman E, Yarin AL, Wendorff JH and Greiner A. Compound core–shell polymer nanofibers by co-electrospinning. *Adv Mater* 2003; 15: 1929–1932.
37. Hong KH. Preparation and properties of electrospun poly(vinyl alcohol)/silver fiber web as wound dressings, *Polym Eng Sci. 2007* 47: 43–49.

38. Uyar T, Havelund R, Hacaloglu J, Besenbacher F and Kingshott P. Functional electrospun polystyrene Nanofibers Incorporating α-, β-, and γ-cyclodextrins: comparison of molecular filter performance. *ACS Nano* 2010; 4: 5121–5130.
39. Supaphol P and Chuangchote S. On the electrospinning of poly(vinyl alcohol) nanofiber mats: a revisit. *J Appl Polym Sci* 2008; 108: 969–978.
40. Ding W, Wei S, Zhu J, Chen X, Rutman D and Guo Z. Manipulated electrospun PVA nanofibers with inexpensive salts. *Macromol Mater Eng* 2010; 295: 958–965.
41. Beachley V and Wen X. Effect of electrospinning parameters on the nanofiber diameter and length. *J Mater Sci Eng. C* 2009; 29: 663–668.
42. Sajeev US, Anand KA, Menon D and Nair S. Control of nanostructures in PVA, PVA/chitosan blends and PCL through electrospinning. *Bull. Mater. Sci* 2008; 31: 343–351.
43. Frenot A and Chronakis IS. Polymer nanofibers assembled by electrospinning. *Curr Opin Colloid Interface Sci* 2003; 8: 64–75.
44. Deitzel JM, Kleinmeyer JD, Hirvonen JK and Beck NC. Controlled deposition of electrospun poly(ethylene oxide) fibers. *Polymer* 2001; 42: 8163–8170.
45. Bognitzki M, Czado W, Frese T, Schaper A, Hellwig M, Steinhart M, Greiner A and Wendorff JH. Nanostructured fibers via electrospinning. *Adv Mater* 2001; 13: 70–72.
46. Reneker DH, Yarin AL, Fong H and Koombhongse S. Bending instability of electrically charged liquid jets of polymer solutions in electrospinning. *J Appl Phys* 2000; 87: 4531–4547.
47. Ojha SS, Afshari M, Kotek R and Gorga RE. Morphology of electrospun nylon-6 nanofibers as a function of molecular weight and processing parameters. *J Appl Polym Sci* 2008; 108: 308–319.
48. Doshi J and Renerker DH. Electrospinning process and applications of electrospun fibers. *J Electrostat* 1995; 35: 151–160.
49. Sukigara S, Gandhi M, Ayutsede J, Micklus M and Ko F. Regeneration of bombyx mori silk by electrospinning-part 1: processing parameters and geometric properties. *Polymer* 2003; 44: 5721–5727.
50. Jin HJ, Fridrikh SV, Rutledge GC and Kaplan DL. Electrospinning bombyx mori silk with poly(ethylene oxide). *Biomacromolecules* 2002; 3: 1233–1239.
51. Ying Y, Jia Z, Liu J, Lei H, Li Q, Wang L and Guan Z. Effect of electric field distribution uniformity on electrospinning. *J Appl Phys* 2008; 103: 104307.
52. Ding B, Kim HY, Lee SC, Shao CL, Lee DR, Park SJ, Kwag GB and Choi KJ. Preparation and characterization of a nanoscale poly(vinyl alcohol) fiber aggregate produced by an electrospinning method. *J Polym Sci, Part B: Polym Phys* 2002; 40: 1261–1268.
53. Zong X, Kim K, Fang D, Ran S, Hsiao BS and Chu B. Structure and process relationship of electrospun bioabsorbable nanofiber membranes. *Polymer* 2002; 43: 4403–4412.
54. Qu L, Peng ZA and Peng X. Alternative routes toward high quality CdSe nanocrystals. *Nano Lett* 2001; 1: 333–337.
55. Scott GWB, Hening JC and Wagstaff A. The flow of cream through narrow glasstubes. *J Phys Chem* 1939; 43: 853–864.
56. Waele O. On the arithmetical representation of viscosity structural fields. *Kolloid Z* 1929; 47: 176–187.
57. Fennessey SF and Farris RJ. Fabrication of aligned and molecularly oriented electrospun polyacrylonitrile nanofibers and the mechanical behavior of their twisted yarns. *Polymer* 2004; 45: 4217–4225.
58. Choi SH, Liu W, Misra P, Tanaka E, Zimmer JP, Ipe IB, Bawendi MG and Frangioni JV. Renal clearance of quantum dots. *Nat Biotech* 2007; 25: 1165–1170.
59. Driel AFV, Allan G, Delerue C, Lodahl P, Vos WL and Vanmaekelbergh D. Frequency-dependent spontaneous emission rate from CdSe and CdTe nanocrystals: Influence of Dark States. *Phys Rev Lett* 2005; 95: 236804.
60. Peppas NA and Merrill EW. Differential scanning calorimetry of crystallized PVA hydrogels. *J Appl Polym Sci* 1976; 20: 1457–1465.
61. Kim MG, Asran SA, Michler GH, Simon P and Kim JS. Electrospun PVA/HAp nanocomposite nanofibers: biomimetics of mineralized hard tissues at a lower level of complexityBioinspir Biomim 2008; 3: 046003.
62. Deschenaux C, Affolter A, Magni D, Hollenstein C and Fayet P. Investigations of CH_4, C_2H_2 and C_2H_4 dusty RF plasmas by means of FTIR absorption spectroscopy and mass spectrometry. *J Phys D: Appl Phys* 1999; 32: 1876–1886.
63. Matveev S, Portnyagin M, Ballhaus C, Brooker R and Geiger CA. FTIR spectrum of phenocryst olivine as an indicator of silica saturation in magmas. *J Petrol* 2005; 46: 603–614.
64. Okuno D, Iwase T, Shinzawa IK, Yoshikawa S and Kitagawa T. FTIR detection of protonation/deprotonation of key carboxyl side chains caused by redox change of the CuA-Heme a moiety and ligand dissociation from the Heme a3-CuB center of bovine heart cytochrome c oxidase. *J Am Chem Soc* 2003; 125: 7209–7218.
65. Sui XM, Shao CL and Liu YC. White-light emission of polyvinyl alcohol/ZnO hybrid nanofibers prepared by electrospinning. *Appl Phys Lett* 2005; 87: 113115–113113.
66. Hellwig P, Behr J, Ostermeier C, Richter O, Pfitzner U, Odenwald A, Ludwig B, Michel H and MÃntele W. Involvement of glutamic acid 278 in the redox reaction of the cytochrome c oxidase from paracoccus denitrificans investigated by FTIR spectroscopy. *Biochemistry* 1998; 37: 7390–7399.
67. Zhu J, Wei S, Zhang L, Mao Y, Ryu J, Haldolaarachchige N, Young DP and Guo Z. Electrical and dielectric properties of polyaniline–Al_2O_3 nanocomposites derived from various Al_2O_3 nanostructures. *J Mater Chem* 2011; 21: 3952–3952.